An Improved Multi-loop Resonant and plug-in Repetitive Control Schemes for Three-Phase Stand-Alone PWM Inverter Supplying Non-Linear Loads

Ahmad Ali Nazeri, and Peter Zacharias
Centre of Competence for Distributed Electric Power Technology
Faculty of Electrical Engineering / Computer Science
University of Kassel, Kassel, Germany
Email: ahmad.nazeri@student.uni-kassel.de, peter.zacharias@uni-kassel.de

August 15, 2022

Acknowledgments

This work was financially supported by the German Academic Exchange Service (DAAD) Germany which provided a fully-funded scholarship to Ahmad Ali Nazeri for sponsoring his doctoral studies.

Keywords

≪Fractional delay≫, ≪Resonant control≫, ≪Repetitive control≫, ≪Total harmonic distortion≫

Abstract

This paper proposes an improved multi-loop control scheme for a three-phase voltage source inverter (VSI) for the island/microgrid operation. The constant voltage constant frequency (CVCF) pulse-width modulation (PWM) inverter can be used to regulate the output voltage with lower total harmonic distortion (THD). The output voltage is regulated under different load conditions, such as linear and rectifier loads for a CVCF for the uninterruptible power supply (UPS) inverter in stand-alone operation. An improved plug-in repetitive controller (RC) with the proportional-resonant (PR) control is used in the outer voltage loop to regulate the output AC voltage, and a simple proportional control is used in the inner current control loop for active damping and improving the transient performance. The instantaneous reference voltage of the converter is used as a feed-forward signal at the output of the converter to robust the system performance and simplify the controller design. This paper proposes a step-by-step design procedure of the voltage and current controllers, an analysis of the overall system stability from the frequency-response viewpoint, and the implementation of the PR with the improved plug-in RC for the three-phase stand-alone inverter supplying linear and nonlinear loads. The improved plug-in RC combined with PR control offers high-quality sinusoidal output voltages, robustness to the parameter uncertainties, fast response, and the need for fewer sensors. Moreover, the modified plug-in RC is effective and simple to be implemented on a digital signal processor (DSP). The three-phase VSI with the proposed multi-loop control is simulated in MATLAB/Simulink and experimentally implemented on a 7.5 kW system on TMDSDOCK28379D 32-bit floating-point DSP from Texas Instruments to validate the excellent steady-state, dynamic and transient performance of the proposed control scheme with better harmonic mitigation.

Introduction

The pulse-width-modulated (PWM) voltage source inverters (VSIs) are extensively integrated into different power conversion applications such as island microgrids, distributed generation, shunt active filters, and uninterruptible power supplies (UPS) [1, 2].

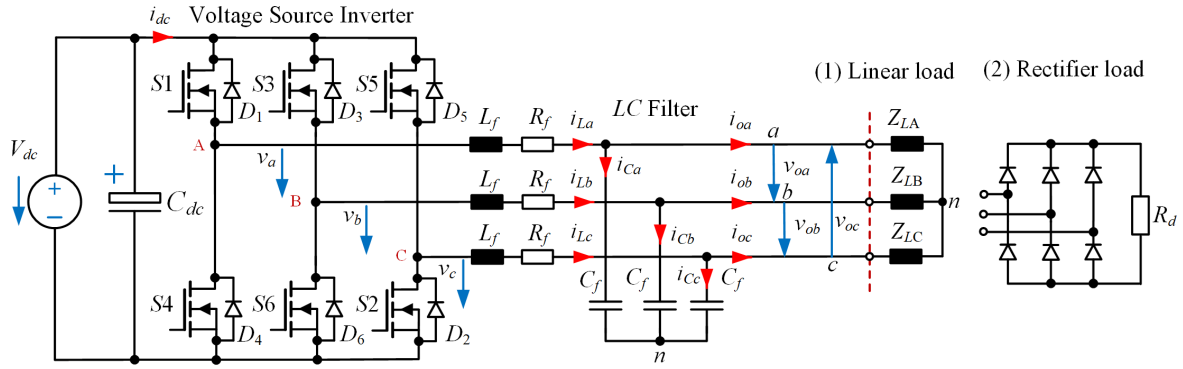

Fig. 1: Three-phase stand-alone inverter

Normally, the PWM VSI is connected to the rectifier loads, which introduces the disturbances into the inverter output voltage and results in the output voltage distortions [2]. Normally, a constant voltage constant frequency (CVCF) PWM inverter is used to achieve constant AC output with low total harmonic distortion (THD) and better transient response [3]. The set control objectives should be attained independent of the distortions caused by the connected load and the inverter. To achieve this, various control approaches have been reported such as deadbeat and model predictive control [4], resonant control [5, 6], and repetitive control (RC) [7, 8]. The RC based on the internal model principle [9], is capable of the perfect tracking of the periodic reference, eliminating the periodic error and has better periodic disturbance capability from the nonlinear load. Conventional RC (CRC) scheme has been extensively adopted in the CVCF PWM inverters [10]. The RC itself is capable of suppressing the odd and even harmonics, but typically it is used with another controller to improve system dynamic performance [11].

The parallel combination of the PR and RC control to mitigate the dead time harmonics with better transient performance in a single-phase PWM grid-connected inverter is analyzed in [12]. A modified RC with a finite impulse response filter (FIR) with the variation in the grid frequency is adopted in [13]. The multi-loop control strategies are normally adopted in the PWM VSIs to regulate the output voltage with nearly zero steady-state error and reduced THD supplying the nonlinear load. The inner current control is used to control the capacitor current or the inverter current for the inverter protection scheme, while the outer voltage control loop is used to track the periodic reference signal and compensate for the harmonics caused by the rectifier load and the nonlinearities of the inverter [14]. This paper proposes the step-by-step design procedure of the PR combined plug-in RC in the voltage loop and a proportional control in the current loop with the system stability analysis. An improved plug-in RC is designed in the discrete-time domain with the variation in the nominal grid frequency with fewer delays. Moreover, the proposed modified RC offers a simple implementation of the DSP with the implementation of the feed-forward loop at the fundamental frequency compared to the CRC. The phase lead compensator z^m is implemented to compensate for the phase lag of the CVCF PWM converter system [15]. A careful design of the improved RC with the lead step z^m is used to compensate for the system phase lag and is capable of eliminating the harmonics, which leads to higher tracking accuracy. Also, the phase lead compensator helps in stabilizing the inverter system with larger gains and results in achieving a fast convergence rate. Experimental results are provided to illustrate the mitigation of the harmonics caused by the nonlinear loads with lower THD and verify the effectiveness of the proposed multi-loop control.

Multi-loop Control System

Fig. 1 depicts the circuit diagram of a three-phase stand-alone CVCF PWM inverter. A constant DC voltage source V_{dc} connected to the three-phase SiC MOSFET with the DC-link capacitor C_{dc} and the current i_{dc}. The inverter is connected to an LC filter L_f, C_f, and the load Z_L. An equivalent resistor R_f presents the damping effects from the inverter losses, dead-time effects, and equivalent series resistance (ESR) of the filter inductance L_f. v_{inv} refers to the inverter output voltage, i_L, i_c and i_o are the inverter, capacitor and load currents respectively where v_o is the output voltage.

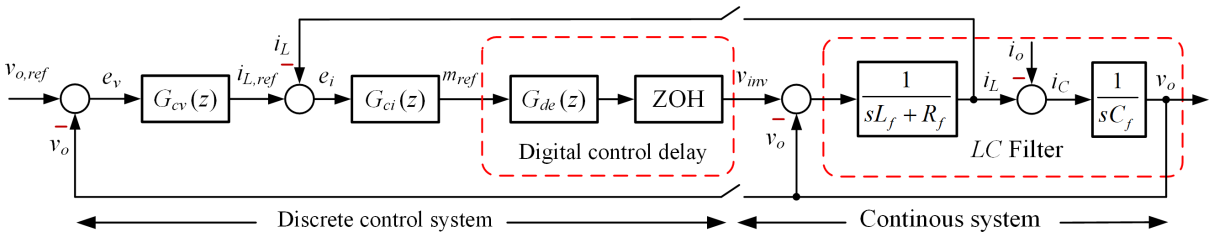

Fig. 2: Conventional multi-loop controller in the stationary reference frame

The VSI can be connected to the linear and/or the diode rectifier load with the output resistive load R_d as shown in Fig. 1. Fig. 2 illustrates the conventional multi-loop controllers for the CVCF PWM inverter in discrete domain [14]. The outer voltage loop $G_{cv}(z)$ regulates the capacitor voltage, $G_{ci}(z)$ is the inverter current feedback control with the inverter protection scheme. The load current i_o can be considered as a disturbance. The $G_{de}(z)$ is the computational and PWM delay. The computational delay is the time period between the sampling instance and the PWM duty cycle. The sampling instant is set to be at the middle of the PWM period, and the duty cycle will be updated at the next sampling instance [15]. The system parameters are listed in Table I. The computational delay is one sampling period T_s and is modeled as in (1) in the z-domain as

$$G_{de}(z) = z^{-1}. \tag{1}$$

The PWM inverter is modeled as a unity gain, and the PWM modulation is treated as a zero-order-hold (ZOH) block with the sampling period delay as shown in Fig. 2. Therefore, one and a half sampling period delay is introduced by the digital [16]. The effect of the digital delay has to be taken into consideration while designing the RC for the CVCF PWM inverter [17]. The open-loop transfer function of the inverter current loop (see Fig. 2) is given as

$$G_{\mathrm{OL},ci}(z) = \frac{i_L}{e_i} = G_{ci}(z)G_{de}(z) \times Z_{\mathrm{ZOH}}\left[\frac{sC_f}{(sL_f + R_f)\,sC_f + 1}\right]. \tag{2}$$

Table I: Inverter system parameters

Parameter	Symbol	Value
Nominal active power	$P_{\max}$	7.5 kW
Base voltage	V_B	325 V
Base current	I_B	15.3 A
Base impedance	Z_B	21.3 Ω
Base capacitance	C_B	150 μF
Output voltage (RMS)	V_{rms}	230 V
DC link voltage	V_{dc}	650 V
Rated output frequency	f_o	50 Hz
Switching frequency	f_{sw}	20 kHz
Sampling frequency	f_s	20 kHz
Computational time delay	T_d	75 μs
Filter inductance	L_f	2.6 mH
Equivalent resistance	R_f	0.1 Ω
Filter capacitance	C_f	6 μF
Connected load	R_d	60 Ω

The closed-loop transfer function of the current feedback control from i_L to $i_{L,ref}$ can be derived as

$$G_{\mathrm{CL},ci}(z) = \frac{i_L}{i_{L,ref}} = \frac{G_{\mathrm{OL},ci}(z)}{1 + G_{\mathrm{OL},ci}(z)}. \tag{3}$$

The inner current control $G_{ci}(z)$ is normally designed as a simple proportional gain [15]. A larger gain of the K_{pi} is needed to force the error to zero, but it should be carefully chosen not to restrict the bandwidth of the voltage control loop. The open-loop transfer function of the voltage control loop can be derived from Fig. 2 as [15]

$$G_{\mathrm{OL},cv}(z) = \frac{v_o}{e_v} = G_{cv}\left[1 - G_{\mathrm{CL},ci}(z)\right] G_{ci}(z) G_{de}(z) \times Z_{\mathrm{ZOH}}\left[\frac{1}{(sL_f + Rf)sC_f + 1}\right]. \tag{4}$$

The closed-loop transfer function of the voltage feedback control v_o to $v_{o,ref}$ can be derived as

$$G_{\mathrm{CL},cv}(z) = H(z) = \frac{v_o}{v_{o,ref}} = \frac{G_{\mathrm{OL},cv}(z)}{1 + G_{\mathrm{OL},cv}(z)}. \tag{5}$$

Equation (5) depicts the precise tracking capability of the proposed multi-loop control system. The $H(z)$ can be derived based on (2)-(5) using the "ZOH" function in MATLAB [15].

Design of the Controllers

Current Control Loop

The inverter current control loop is designed in the stationary reference frame ($\alpha\beta$) using only a proportional gain of K_{pi}. A PI controller in a synchronous reference frame (dq) can also be used in the current control loop, but it introduces undesirable phase delay. The objective of using a proportional gain is to achieve proper resonance damping, and the reference voltage feed-forward path in the control scheme can be added at the output of the converter system to reduce the steady-state error, and the complexity of the controller design [18]. The open-loop transfer function of the current loop in the continuous domain, which is similar to the discrete domain in (2) and shown in Fig. 2 is given as

$$G^s_{\mathrm{OL},ci}(s) = G^s_{\mathrm{PR}_{ci}}(s) G_{fi}(s) = \underbrace{\left(K_{pi} + \frac{K_i s}{s^2 + \omega_o^2}\right)}_{\text{PR current controller}} \underbrace{\left(\frac{V_{dc}}{sL_f + R_f}\right)}_{\text{Inverter}}. \tag{6}$$

where $'s'$ denotes the SRF, K_i is the integral gain of the current controller, and ω_o is the nominal frequency. The closed-loop transfer function of the current control is expressed as [16]

$$\begin{aligned} G^s_{\mathrm{CL},ci}(s) &= \frac{G^s_{\mathrm{PR}_{ci}}(s) G_{fi}(s)}{1 + G^s_{\mathrm{PR}_{ci}}(s) G_{fi}(s)} \\ &= \frac{\frac{V_{dc}}{L_f}\left(K_{pi}s^2 + K_i s + K_{pi}\omega_o^2\right)}{s^3 + \frac{1}{L_f}\left(K_{pi}V_{dc} + R_f\right)s^2 + \left(\omega_o^2 + \frac{K_i V_{dc}}{L_f}\right)s + \frac{\omega_o^2}{L_f}\left(K_{pi}V_{dc} + R_f\right)}. \end{aligned} \tag{7}$$

The third-order closed-loop characteristic equation is compared to the Naslin characteristic polynomial equation to extract the current control parameters as given as

$$P_N(s) = a_0\left(1+\frac{s}{w_0}+\frac{s^2}{\alpha w_0^2}+\frac{s^3}{\alpha^3 w_0^3}\right) = \frac{a_0}{\alpha^3 w_0^3}\left(\alpha^3 w_0^3+\alpha^3 w_0^2 s+\alpha^2 w_0 s^2+s^3\right). \tag{8}$$

where w_0 is the pulsation, and the damping factor ζ is related to the value of α

$$\zeta = \frac{\alpha-1}{2}. \tag{9}$$

The following relation holds after the comparison of the closed-loop current control (7) with the Naslin polynomial (8) as expressed as

$$\begin{aligned} \alpha^2 w_0 &= \frac{1}{L_f}\left(K_{pi}V_{dc}+R_f\right), & \alpha^3 w_0^2 &= \omega_o^2+\frac{K_i V_{dc}}{L_f}, \\ \alpha^3 w_0^3 &= \frac{\omega_o^2}{L_f}\left(K_{pi}V_{dc}+R_f\right), & a_0 &= \alpha^3 w_0^3. \end{aligned} \tag{10}$$

The pulsation w_0 is derived from (10) as

$$w_0 = \frac{\omega_o}{\sqrt{\alpha}}. \tag{11}$$

which then leads to the parameters of the PR current control loop as [16]

$$K_{pi} = \frac{\alpha\sqrt{\alpha}\omega_o L_f - R_f}{V_{dc}}, \qquad K_i = \frac{\omega_o^2 L_f\left(\alpha^2-1\right)}{V_{dc}}. \tag{12}$$

Voltage Control Loop

The fundamental component of the PR controller can be used in parallel with the resonant-harmonic compensators (RHCs) to mitigate the low-order harmonics [5, 6]. Fig. 3a shows the PR in parallel with the RHCs in the voltage control loop to reduce the voltage harmonics when the rectifier load is connected. The open-loop transfer function of the voltage control loop in $\alpha\beta$ frame can be determined as

$$G^s_{\mathrm{PR},cv}(s) = \frac{i_{L,ref}(s)}{e_v(s)} = \underbrace{K_{pv}+\frac{K_{iv}s}{s^2+\omega_o^2}}_{1^{\mathrm{st}}\text{harmonic}} + \underbrace{\sum_n \frac{K_{ivn}s}{s^2+(n\omega_o)^2}}_{n^{\mathrm{th}}\text{harmonic}}. \tag{13}$$

where K_{pv} is proportional, and K_{ivn} is the integral gain of each RHCs with n being 3, 5, 7, etc. The PR controller is used for the capacitor voltage control design in the $\alpha\beta$ frame. The open-loop transfer function of the voltage control loop is given as [16]

$$G^s_{\mathrm{OL},cv}(s) = G^s_{\mathrm{PR}_{cv}}(s)G_{fv}(s) = \underbrace{\left(K_{pv}+\frac{K_{iv}s}{s^2+\omega_o^2}\right)}_{\text{PR voltage controller}}\underbrace{\left(\frac{1}{sC_f}\right)}_{\text{Filter capacitor}}. \tag{14}$$

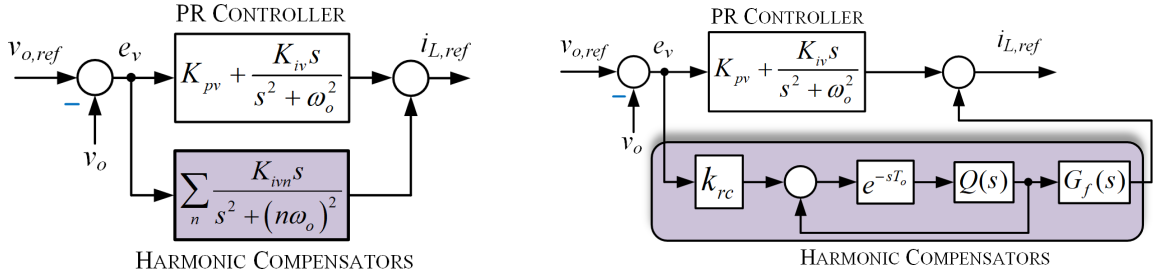

Fig. 3: Block diagram of the voltage control loop (a) PR controller with RHCs. (b) PR controller in parallel with RC

The closed-loop transfer function of the voltage loop is given as

$$G^s_{\mathrm{CL},cv}(s) = \frac{G^s_{\mathrm{PR}_{cv}}(s)G_{fv}(s)}{1+G^s_{\mathrm{PR}_{cv}}(s)G_{fv}(s)} = \frac{\frac{1}{C_f}\left(K_{pv}s^2+K_{iv}s+K_{pv}\omega_o^2\right)}{s^3+\frac{K_{pv}}{C_f}s^2+\left(\frac{K_{iv}}{C_f}+\omega_o^2\right)s+\frac{K_{pv}\omega_o^2}{C_f}}. \tag{15}$$

Comparing the closed-loop transfer function $G^s_{\mathrm{CL},cv}(s)$ in (15) to (8), the controller parameters for the voltage loop can be extracted in similar fashion as explained in (10) and (11), which are expressed as

$$\begin{aligned} \alpha^2 w_0 &= \frac{K_{pv}}{C_f}, & \alpha^3 w_0^2 &= \frac{K_{iv}}{C_f}+\omega_o^2, \\ \alpha^3 w_0^3 &= \frac{K_{pv}\omega_o^2}{C_f}, & a_0 &= \alpha^3 w_0^3. \end{aligned} \tag{16}$$

which then leads to the parameters of the PR voltage control loop as [16]

$$K_{pv} = \omega_o C_f \sqrt{\alpha^3}, \qquad K_{iv} = \omega_o^2 C_f\left(\alpha^2-1\right). \tag{17}$$

An Improved plug-in Repetitive Control Loop

According to the internal model principle [9], the output of the closed-loop system can track and reject the reference and disturbance signal respectively with zero steady-state error if the accurate model is included in the closed-loop system. Fig. 3b shows the PR controller in parallel with the repetitive controller for better transient performance and harmonic compensation [5, 8, 12]. The open-loop transfer function of the RC harmonic compensator $G_{\mathrm{RC}}(s)$ for the voltage loop as shown in Fig. 3b in continuous domain can be expressed as

$$G^s_{\mathrm{OL},cv}(s) = \frac{i_{L,ref}(s)}{e_v(s)} = G^s_{\mathrm{PR}cv}(s) + \underbrace{k_{rc}\frac{e^{-sT_o}Q(s)G_f(s)}{1-e^{-sT_o}Q(s)}}_{\mathrm{G_{RC}}(s)} \tag{18}$$

where k_{rc} is the RC gain, which can be selected between $0 < k_{rc} < 2$, $\omega_o = 2\pi/T_o$ is the fundamental frequency, and T_o is the fundamental period. A low-pass filter LPF $Q(s)$ is included in the RC compensator to attenuate high-order harmonics and lead to the stability of the controller [11] but it might degrade the tracking capability of the controller. The $Q(s)$ can be presented in the z-domain as

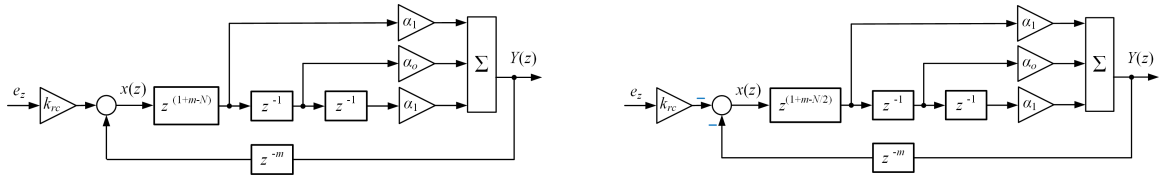

(a) Even/odd harmonic repetitive control (b) Odd harmonic repetitive control

Fig. 4: Discrete-time implementation of the improved repetitive control

$$Q(z) = \alpha_1 z + \alpha_0 + \alpha_1 z^{-1}. \tag{19}$$

where $2\alpha_1 + \alpha_1 = 1$, $\alpha_1 > 0$, and $\alpha_0 > 0$. The design of the LPF can be done by examining the harmonic content of the voltage controlled by the PR controller. Moreover, $G_f(s)$ is a phase-lead compensator, which is also considered in the closed-loop system stability. The phase-lead step is given as

$$G_f(z) = z^m. \tag{20}$$

where m is the phase-lead number, determined using the trial and error method during the experiments. The RC with the LPF and the phase-lead compensator can be implemented in a digital microprocessor using cascaded delays. The ideal RC in (18) with $Q(s) = 1$ and $G_f(s) = 1$ can be expanded as

$$G_{\mathrm{RC}}(s) = k_{rc}\left[-\frac{1}{2} + \frac{1}{T_o s} + \frac{2}{T_o}\left(\sum_{n}^{\infty} \frac{s}{s^2 + (n\omega_o)^2}\right)\right]. \tag{21}$$

where $n = 1, 2, 3, ..$ is the harmonic order including the fundamental component [12]. For practical implementation, the improved RC in (18) can be expressed in z-domain as

$$G_{\mathrm{RC}}(z) = k_{rc}\frac{z^{-N}Q(z)G_f(z)}{1 - z^{-N}Q(z)}. \tag{22}$$

where $N = f_s T_o$ is the number of samples in one repetitive period, and f_s is the sampling frequency. Typically, $n \leq N_f$, where $N_f = f_s T_o/2$ is the Nyquist frequency. The RC scheme can compensate the harmonics up to the Nyquist frequency, since it contains N_f individual RHCs in parallel [12]. Fig. 4 shows the improved discrete implementation of the repetitive control for even/odd (N) harmonics (see Fig. 4a) and odd harmonics (N/2) (see Fig. 4b) realized on a DSP. The discrete transfer function of the RC output $Y(z)$ to the input $e(z)$ is given as

$$\frac{Y(z)}{e(z)} = \underbrace{k_{rc}\frac{z^{-N}Q(z)G_f(z)}{1 - z^{-N}Q(z)}}_{\text{Even/odd harmonics } \mathrm{G_{RC}}(z)}, \qquad \frac{Y(z)}{e(z)} = -\underbrace{k_{rc}\frac{z^{-N/2}Q(z)G_f(z)}{1 + z^{-N/2}Q(z)}}_{\text{Odd harmonics } \mathrm{G_{RC}}(z)}. \tag{23}$$

The improved repetitive controller in (22) and shown in Fig. 4a is used for the three-phase stand-alone VSI. Substituting (19) into (22) and rearranging results in

$$Y(z) = x(z)\left(\alpha_1 z^{1+m-N} + \alpha_0 z^{m-N} + \alpha_1 z^{m-N-1}\right). \tag{24}$$

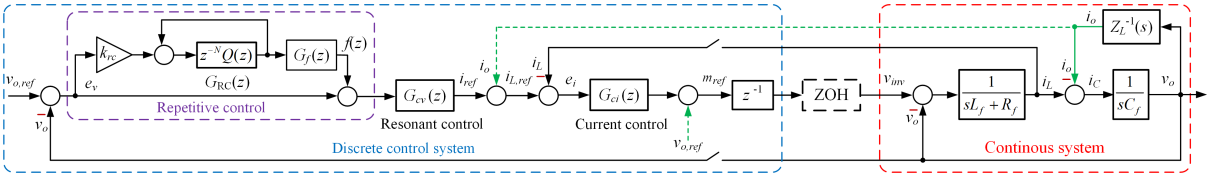

Fig. 5: The proposed improved multi-loop PR plug-in RC with the control scheme of the whole system in the stationary reference frame

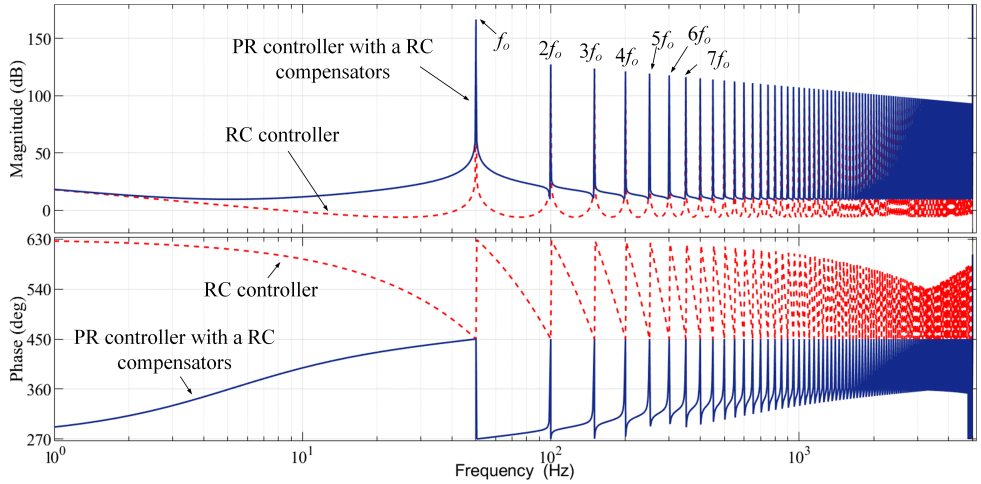

(a)

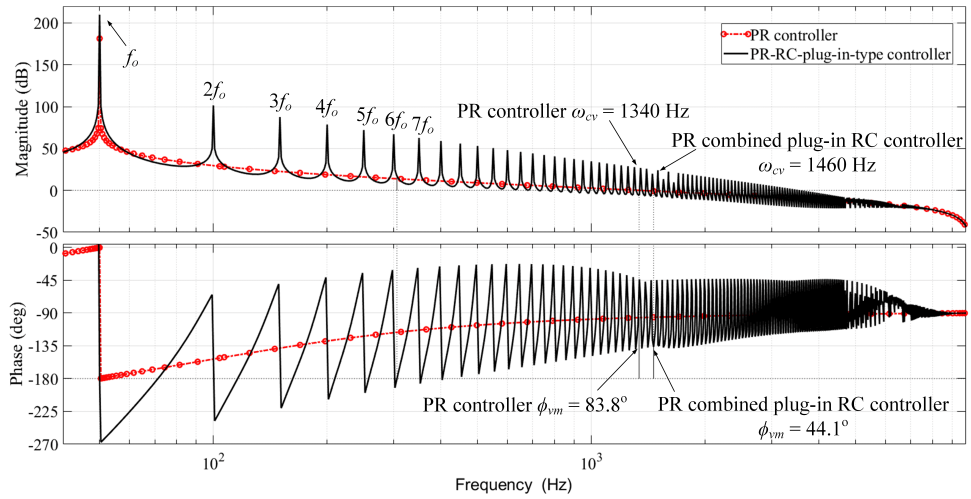

(b)

Fig. 6: Frequency response of the open-loop voltage control in stationary reference frame: (a) PR in parallel with RC controller as a harmonic compensator; (b) Improved PR combined plug-in RC controller

where $x(z)$ is given by

$$x(z) = e(z)k_{rc} + z^{-m}Y(z). \tag{25}$$

Equations (24) and (25) are the standard realization of the controller and shown in Fig. 4a. The overall improved multi-loop PR plug-in RC of the system is illustrated in Fig. 5. The plug-in type RC is given in purple dashed as shown in Fig. 5.

Table II: Parameters of the proposed control system

Parameter	Symbol	Value
Current loop proportional gain	K_{pi}	1.28
Voltage loop proportional gain	K_{pv}	0.91
Voltage loop integral gain	K_{iv}	795
Resonant controller frequency	ω_o	314
Controller value	α	3
Damping factor	ζ	0.95
Repetitive controller gain	k_{rc}	0.98
LPF $Q(z)$ coefficients	α_0, α_1	0.25, 0.5
Phase-lead compensator	$G_f(z)$	z^3
Delay line	$N = f_s/f_o$	400

The feed-forward reference voltage can also be added for better transient response and avoids the phase delay in the control system. Moreover, the load current i_o can also be used as a feedback control signal for a better transient and steady-state performance and provides better inverter protection as shown in Fig. 5 [6, 14]. The open-loop transfer function of the voltage control in z-domain for the parallel and plug-in type RC control with the PR control is given as

$$G_{\mathrm{OL},cv}(z) = G_{\mathrm{PR}cv}(z) + G_{\mathrm{RC}}(z) \times G_{fv}(z) \qquad \rightarrow [\mathrm{Parallel-type}] \tag{26a}$$

$$G_{\mathrm{OL},cv}(z) = G_{\mathrm{PR}cv}(z) \times (1 + G_{\mathrm{RC}}(z)) \times G_{fv}(z). \qquad \rightarrow [\mathrm{Plug-in-type}] \tag{26b}$$

Fig. 6 is extracted from (26) with the proposed control parameters given in Table II. Fig. 6a is the open-loop frequency response of the parallel combination of the RC and PR control (see 26a) where Fig. 6b is the improved plug-in RC combined with PR control (see 26b) in the $\alpha\beta$ frame. Fig. 6a and (21) shows that the RHCs can approach an infinite gain at the corresponding resonant frequency $n\omega_o$. Moreover, the PR control with the parallel and/or plug-in type combination of RC harmonic compensator can suppress all harmonics up to the Nyquist frequency as presented in Fig. 6. The cross-over frequency ω_{cv} for the PR and PR combined with the plug-in type RC control is 81490 rad/s and 91735 rad/s respectively. Moreover, the phase margin ϕ_{vm} for the PR and PR combined with the plug-in type RC control is 83.8^{o} and 44.1^{o} respectively as illustrated in Fig. 6b, which is still high enough for the closed-loop stability of the voltage control.

Experimental Verification

The simulation and experimental results were extracted by implementing the three-phase VSI system as illustrated in Fig. 1. The detailed system and proposed control parameters used for the simulation and experiments are listed in Table I and II respectively. The three-phase VSI system shown in Fig. 1 with the proposed control in Fig. 5 were implemented with the space vector modulation (SVM) in MATLAB/Simulink. The multi-loop control scheme shown in Fig. 5 with the improved PR combined plug-in RC in the voltage loop and a proportional control in the current loop was implemented. The base voltage V_B, base current I_B, base impedance Z_B, and the base capacitance C_B given in Table I were used to calculate the control parameters in the per-unit system, and the measured voltages and currents were scaled into the per-unit system for the simulation and experiments. The PR control was discretized and implemented using the forward and backward Euler method and the modified plug-in RC control depicted in Fig. 4a was implemented using (24) and (25) with the control parameters given in Table II.

Fig. 7 illustrates the laboratory setup for the implementation of the proposed PR combined plug-in RC control scheme. The prototype includes a constant DC source V_{dc} using the programmable DC power source from the Regatron, a three-phase inverter constructed from the CoolSiC MOSFET, an *LC* filter,

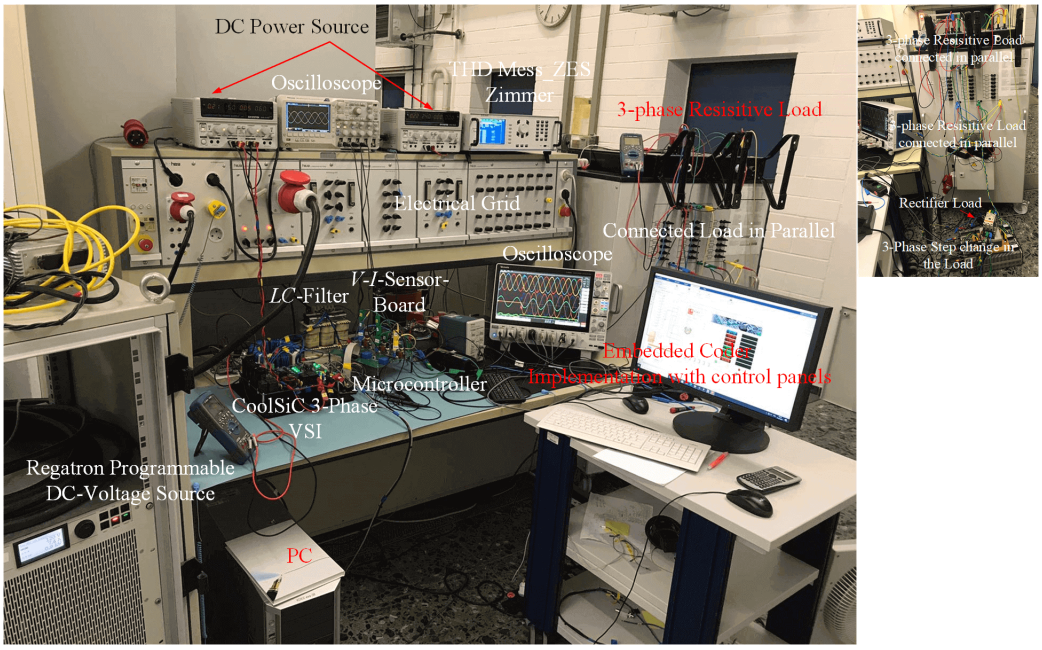

Fig. 7: Laboratory setup for the three-phase stand-alone inverter with an *LC* filter and connected linear and rectifier loads

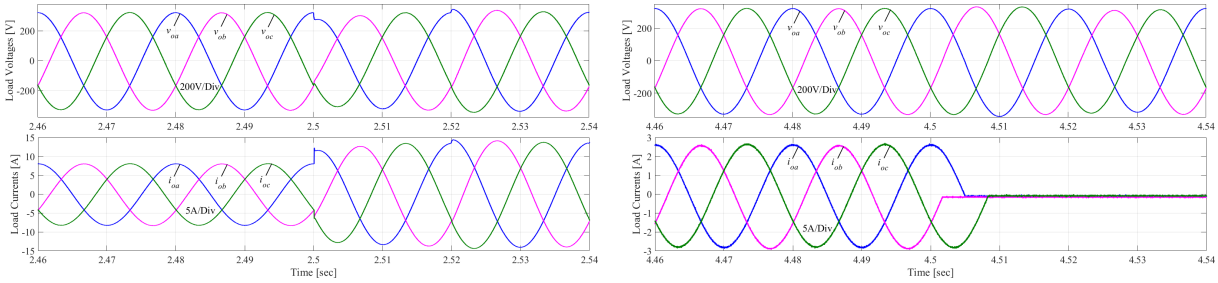

(a) (b)

Fig. 8: Experimental transient results of the three-phase VSI with the step-change in the load with PR combined plug-in RC control; (a) half-load to full load, (b) half-load to no-load

a three-phase voltage and current sensors, and a DSP control board with sampling circuits. The voltage and current THDs and the results were extracted from the precision power analyzer ZES-Zimmer and an 8-channel MSO68B oscilloscope respectively as shown in Fig. 7. The reference signals $V_{\alpha,ref}$ and $V_{\beta,ref}$ are the input signals to the SVM to generate the control signals. The discrete control schemes were implemented on a TMDSDOCK28379D 32-bit floating-point DSP controller from Texas Instruments. The internal signals of the discrete control scheme implemented on the DSP were converted to 0-3.0 V analog signals via two embedded 12-bit digital-to-analog converters (DACs) and displayed on the oscilloscope. The analog signal sampling was performed in the middle of every switching period T_s. Fig. 8 illustrates the experimental results of the step-change in the resistive load using the PR combined plug-in RC control. Fig. 8a shows the step-change from half-load to full-load where Fig. 8b depicts the dynamic performance of the system from half-load to no-load. It can be seen that the proposed control is faster to the step-changes in the load and the output voltage is constant. Fig. 9 shows the experimental results of the improved PR combined plug-in RC control when highly nonlinear load is connected at the output. Fig. 9a and Fig. 9b illustrates the transient performance of the system with and without proposed plug-in RC control respectively. The proposed PR combined plug-in RC control has superior performance under rectifier load compared to the standard PR control. Also, the THD of the suggested PR combined RC control is 0.46 % compared to the 9.84 % when only PR control is implemented with the current THD of 30 %.

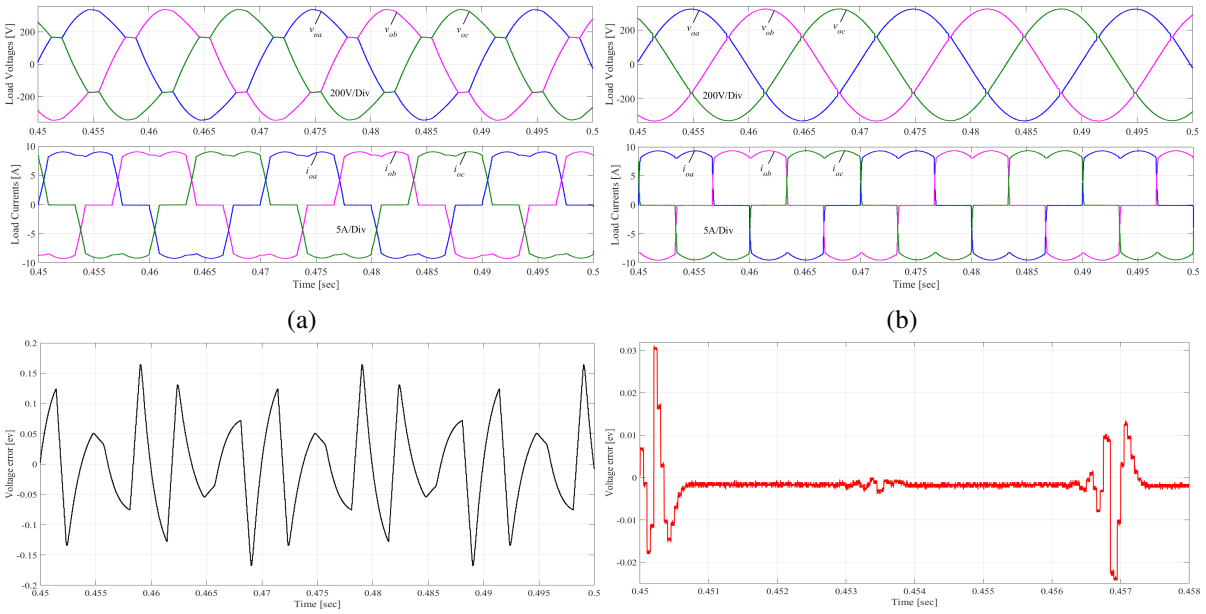

Fig. 9: Experimental dynamic performance of the three-phase VSI under rectifier load; (a) only PR control, (b) improved PR combined plug-in RC control (c) the voltage control loop error e_v with only PR control, (d) the voltage control loop error e_v with improved PR combined plug-in RC control

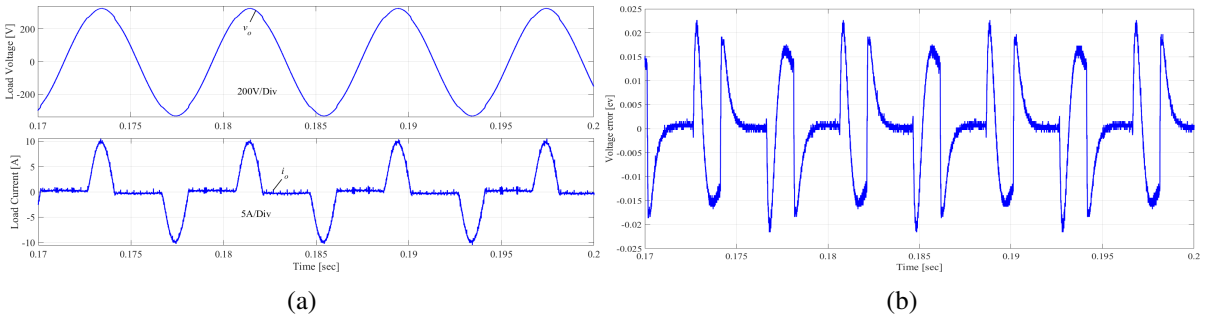

Fig. 10: Experimental performance of the single-phase VSI under nonlinear load with improved PR combined plug-in RC control; (a) output (v_o, i_o), (b) the voltage control loop error e_v

Moreover, the voltage control loop error e_v ($v_{o,ref} - v_o$) under nonlinear load with and without modified plug-in RC control can be seen in Fig. 9c and Fig. 9d respectively. Fig. 10 illustrates the experimental results of the single-phase inverter with the proposed improved PR combined plug-in RC control under highly nonlinear load conditions. Fig. 10a depicts the output voltage and current without the load current feedback (LCF) where Fig. 10b shows the voltage control loop error e_v.

Conclusion

This paper presents an improved PR combined plug-in repetitive control scheme capable to suppress the current harmonics caused by the rectifier loads at the output of the VSI-based islanded microgrid system. A step-by-step design procedure of the voltage and current control loop in $\alpha\beta$ frame is presented. The PR control combined plug-in RC control is implemented in the voltage control loop and the proportional control in the current loop considering the sampling and computational delay. The discrete PR combined RC control is simple in structure without the need for extra load current sensors. The proposed control scheme has higher system stability with maximum phase margin, better tracking accuracy, and better disturbance rejection capability. The output voltage presents a lower THD of 0.46% with the load current THD of 30% and without the need of the load current feedback when the nonlinear load is connected.

Also, the proposed PR combined plug-in RC control offers almost zero steady-state error, fast error convergence, and better dynamic and transient performance compared to the standard control. Moreover, the proposed control mechanism presents a simple implementation on a DSP system by implementing a feed-forward loop at the fundamental frequency that the voltage is bounded during the convergence period of the RC compared to the implementation of the traditional long delay feature of the RC. The load current feedback can also be used for better transient performance but it increases the cost of the overall system.

References

[1] R. Wai, C. Lin, Y. Huang and Y. Chang, "Design of High-Performance Stand-Alone and Grid-Connected Inverter for Distributed Generation Applications," IEEE Transactions on Industrial Electronics, vol. 60, no. 4, pp. 1542-1555, 2013.

[2] A. A. Nazeri, P. Zacharias, F. M. Ibanez and I. Idrisov, "Paralleled Modified Droop-Based Voltage Source Inverter for 100% Inverter-Based Microgrids," 2021 IEEE Industry Applications Society Annual Meeting (IAS), 2021, pp. 1-8, 2021.

[3] T. Yokoyama and A. Kawamura, "Disturbance observer based fully digital controlled PWM inverter for CVCF operation," IEEE Transactions on Power Electronics, vol. 9, no. 5, pp. 473-480, 1994.

[4] S. Kouro, P. Cortes, R. Vargas, U. Ammann and J. Rodriguez, "Model Predictive Control—A Simple and Powerful Method to Control Power Converters," IEEE Transactions on Industrial Electronics, vol. 56, no. 6, pp. 1826-1838, 2009.

[5] Teodorescu, Remus, Frede Blaabjerg, Marco Liserre, and P. Chiang Loh. "Proportional-resonant controllers and filters for grid-connected voltage-source converters." IEE Proceedings-Electric Power Applications, vol. 153, no. 5, 750-762, 2006.

[6] Somkun, Sakda. "Unbalanced synchronous reference frame control of singe-phase stand-alone inverter." International Journal of Electrical Power & Energy Systems, vol. 107, pp. 332-343, 2019.

[7] S. Jiang, D. Cao, Y. Li, J. Liu and F. Z. Peng, "Low-THD, Fast-Transient, and Cost-Effective Synchronous-Frame Repetitive Controller for Three-Phase UPS Inverters," IEEE Transactions on Power Electronics, vol. 27, no. 6, pp. 2994-3005, 2012.

[8] A. Lidozzi, C. Ji, L. Solero, P. Zanchetta and F. Crescimbini, "Resonant–Repetitive Combined Control for Stand-Alone Power Supply Units," IEEE Transactions on Industry Applications, vol. 51, no. 6, pp. 4653-4663, 2015.

[9] Francis, Bruce A., and William M. Wonham. "The internal model principle for linear multivariable regulators, Applied mathematics and optimization," vol. 2, no. 2, pp. 170-194, 1975.

[10] Kai Zhang, Yong Kang, Jian Xiong and Jian Chen, "Direct repetitive control of SPWM inverter for UPS purpose," IEEE Transactions on Power Electronics, vol. 18, no. 3, pp. 784-792, 2003.

[11] Nazir, R., Zhou, K., Watson, N. and Wood, A., "Analysis and synthesis of fractional order repetitive control for power converters." Electric Power Systems Research, vol. 124, pp. 110-119, 2015.

[12] Y. Yang, K. Zhou, H. Wang and F. Blaabjerg, "Analysis and Mitigation of Dead-Time Harmonics in the Single-Phase Full-Bridge PWM Converter With Repetitive Controllers," IEEE Transactions on Industry Applications, vol. 54, no. 5, pp. 5343-5354, 2018.

[13] D. Chen, J. Zhang and Z. Qian, "An Improved Repetitive Control Scheme for Grid-Connected Inverter With Frequency-Adaptive Capability," IEEE Transactions on Industrial Electronics, vol. 60, no. 2, pp. 814-823, 2013.

[14] Poh Chiang Loh, M. J. Newman, D. N. Zmood and D. G. Holmes, "A comparative analysis of multiloop voltage regulation strategies for single and three-phase UPS systems," IEEE Transactions on Power Electronics, vol. 18, no. 5, pp. 1176-1185, 2003.

[15] S. Yang, P. Wang, Y. Tang and L. Zhang, "Explicit Phase Lead Filter Design in Repetitive Control for Voltage Harmonic Mitigation of VSI-Based Islanded Microgrids," IEEE Transactions on Industrial Electronics, vol. 64, no. 1, pp. 817-826, 2017.

[16] Bacha, Seddik, Iulian Munteanu, and Antoneta Iuliana Bratcu. "Power electronic converters modeling and control." Advanced textbooks in control and signal processing, vol 454, no. 454, 2014.

[17] A. A. Nazeri, P. Zacharias, F. M. Ibanez and S. Somkun, "Design of Proportional-Resonant Controller with Zero Steady-State Error for a Single-Phase Grid-Connected Voltage Source Inverter with an LCL Output Filter," 2019 IEEE Milan PowerTech, pp. 1-6, 2019.

[18] M. Monfared, S. Golestan and J. M. Guerrero, "Analysis, Design, and Experimental Verification of a Synchronous Reference Frame Voltage Control for Single-Phase Inverters," IEEE Transactions on Industrial Electronics, vol. 61, no. 1, pp. 258-269, 2014.